Article

Materials mutualism through EDLC behaved MWCNTs with pseudocapacitive MoTe2 nanopebbles: Enhanced supercapacitive performance

Swapnil S Karade, and Babasaheb R Sankapal

ACS Sustainable Chem. Eng., **Just Accepted Manuscript** • DOI: 10.1021/acssuschemeng.8b03366 • Publication Date (Web): 02 Oct 2018

Materials mutualism through EDLC behaved MWCNTs with pseudocapacitive $MoTe_2$ nanopebbles: Enhanced supercapacitive performance

Swapnil S. Karade, Babasaheb R. Sankapal*

Nanomaterials and Device Laboratory, Department of Physics, Visvesvaraya National Institute of Technology, Nagpur- 440010, Maharashtra (India)

*Corresponding Author

Dr. Babasaheb R. Sankapal

Email: brsankapal@phy.vnit.ac.in, brsankapal@gmail.com

Contact No. : + 91(712)2801170: Fax No.: + 91(712)2223230

Abstract

Present innovation emphasis on the design and development of hybrid nanoarchitecture by using simple two step chemical routes; namely 'dip and dry' for multiwalled carbon nanotubes (MWCNTs) followed by coating of molybdenum telluride ($MoTe_2$) nanopebbles using successive ionic layer adsorption and reaction (SILAR) to form thin film onto flexible stainless steel (SS) substrate towards the fabrication of symmetric solid-state and flexible supercapacitor device. The MWCNTs/$MoTe_2$ nanostructured composite exhibits strong synergy and materials mutualism between electric double layer capacitive (EDLC) behaved MWCNTs with pseudocapacitive $MoTe_2$ leading to the enhanced supercapacitive performance. Interestingly, formed unique nanoarchitecture offers excellent charge-storing capability of 502 F/g as specific capacitance at 2 mV/s in liquid configuration with excellent rate capability and cyclic stability. Formed flexible complete solid-state symmetric supercapacitor (FCSS-SC) device using two SS/MWCNTs/$MoTe_2$ electrodes with polyvinyl alcohol-lithium perchlorate (PVA-$LiClO_4$) gel electrolyte as a mediator has demonstrated upgraded potential window resulting in superior capacitance and energy density. Additionally, mechanical flexibility, cyclic stability and hands on application by glowing light emitting diode (LED) can attract the value of formed device towards the advanced energy storage meadow.

Keywords: EDLC:MWCNTs; Pseudocapacitive:$MoTe_2$; Nanocomposite; Solid-state supercapacitor

Introduction

Mutualism is the symbiotic relation between two entities in which composite gains advantages of individual one. The development of multifaceted material structure is the important tool in order to improve the device storage capability. Truly, carbon based materials namely; carbon nanotubes (CNTs), graphene, reduced graphene oxide (rGO) and activated carbon exhibits electric double layer capacitive (EDLC) behavior with long term stability, less degradation and high surface area, but suffer through low specific capacitances. Contrary, nanostructured inorganic metal oxides, hydroxides, and chalcogenides shows pseudocapacitive (faradaic reversible) charge storage behavior with enhanced specific capacitance but, limits its applicability due to degradation of active electrode material which diminishes the life cycle of the supercapacitor (SC) device. Hence, formation of composite can overcome the limitations of individuals ones, by combining pseudocapacitive material having higher specific capacitance with high surface area EDLC material having higher cyclic stability. Therefore, present state of art includes 'materials mutualism' where supercapacitive performance has been enhanced drastically due to formation of nanocomposite by using EDLC behaved MWCNTs with pseudocapacitive $MoTe_2$.

Recently, metal chalcogenides (MX_2= M-Metals and X-S, Se, Te) have gained much interest in nano-world due to their availability, simple way of synthesis and less toxicity along with the physico-chemical properties[1-6]. Depending upon the optical, electrical, chemical and mechanical properties, the metal chalcogenides have been employed for wide variety of applications including solar cell, photocatalysis, hydrogen evolution, batteries, supercapacitor and field emission etc. As far as metal chalcogenides is concern, metal sulfides have been more highlighted for energy storage application. In last decade, metal selenides come forward with admirable potential in the field of energy storage and conversion. Zhang et al.[7] have used highly stable SnSe-nanosheets and $SnSe_2$-nanodisks

through one-pot chemical route for flexible solid-state symmetric supercapacitor with exceptional supercapacitive performance. Also, self-templated synthesized nitrogen doped $CoSe_2$/C double-shelled dodecahedra have been successfully used for high performance supercapacitors[8]. Furthermore, Tang et al. reported the simple one-step hydrothermal route to synthesize NiSe nanowire over nickel foam as a novel binder-free electrode material for supercapacitor which yields 1790 F/g specific capacitance[9]. In addition, $(NiCo)_{0.85}Se$ as a ternary metal selenide has been utilized as a positive electrode for the fabrication of asymmetric device with graphene as negative electrode[10]. Such asymmetric combination of $(NiCo)_{0.85}Se$//graphene has exhibited as wide potential window of 1.8 V with outstanding energy density of 2.85 mWh/cm^3.

In particular, molybdenum based chalcogenides (MoX_2, X=S, Se, Te) specify their identity through simple synthesis, eco-friendly nature, environmental abundance, and most importantly, its application in energy storage and conversion[11-15]. Till date, evolving literature is available on MoS_2 and $MoSe_2$ whereas a very few reports are emerged on $MoTe_2$ as a supercapacitor in energy storage devices even though they have better electrical properties along with semi-metallic nature. Such properties facilitate better access for electrons transfer and provide less electric series resistance. Merely, Liu and co-workers utilize these properties in positive way towards supercapacitor application and successfully obtained specific capacitance of 1393 F/g for chemical vapor deposited 1T'-$MoTe_2$ ultrathin nanosheet[13]. They have extended their efforts towards the fabrication of asymmetric device using 1T'-$MoTe_2$//activated carbon and interestingly obtained specific capacitance of 159 F/g with an energy density of 56.4 Wh/kg. Whereas, graphene supported lamellar 1T'-$MoTe_2$ successfully yields 1.5 fold increment in specific capacitance than bare 1T-$MoTe_2$ electrode[16].

Present state of art deals with the utilization of 'materials mutualism' through the effective combination of MWCNTs nanonetwork anchored with $MoTe_2$ nanopebbles in thin film form onto stainless steel (SS) substrate towards the development of symmetric solid-state supercapacitor device with the following steps: (i) 'Dip and dry' coating of MWCNTs thin film with high surface area onto flexible SS substrate, , (ii) Direct growth of $MoTe_2$ orbicular nanopebbles onto MWCNTs by using the simple, cost efficient and binder free successive ionic layer adsorption and reaction (SILAR) method, (iii) Electrochemical study of individual SS/MWCNTs and SS/$MoTe_2$ followed by hybrid SS/MWCNTs/$MoTe_2$ thin film electrodes by using conventional three electrode system in aqueous NaOH electrolyte, and (iv) Design and supercapacitive performance of a symmetric solid-state supercapacitor device based on SS/MWCNTs/$MoTe_2$//$MoTe_2$/MWCNTs/SS sandwich structure with PVA-$LiClO_4$ gel electrolyte as a mediator.

Experimental

Synthesis of SS/$MoTe_2$ and SS/ MWCNTs /$MoTe_2$ hybrid thin films

Well optimized reported conditions have been taken into consideration to deposit MWCNTs thin film (Supporting Information, S1) onto SS substrate to form SS/MWCNTs[17]. In the present work, $MoTe_2$ thin films have been deposited onto SS and SS/MWCNTs by using SILAR method which is based on alternate immersion of the substrates in separately placed cationic and anionic precursors at room temperature (27 ºC). In brief, i) beaker A contains 0.025 M ammonium molybdate solution complexed with 1 M citric acid and 1 ml solution of 1% sodium borohydrate as reducing agent, ii) beaker B contain double distilled water (DDW) in order to remove loosely bound cations, iii) beaker C contains 0.05 M sodium tellurite as an anionic precursor with 1 ml of 1% sodium borohydtate solution as reducing agent, and iv) beaker D contain DDW in order to remove loosely bound powdery particles or unreacted

species. The sequential immersion of SS and pre-coated SS/MWCNTs substrates in the respective A, B, C and D beakers containing solutions were performed with the time interval of 20, 10, 20 and 10 seconds, respectively, and the process was repeated 20 times to get the terminal thickness of $MoTe_2$ thin layer. Scheme 1 presents the process involved in the development of SS/MWCNTs, SS/$MoTe_2$ and SS/MWCNTs/$MoTe_2$ hybrid thin film. The samples were characterized by using different characterization techniques (Supporting Information, S2).

Results and discussion

Reaction kinetics

Ammonium heptamolybdate as a source of Mo-ions has been complexed with citric acid (CA) to obtain Mo^{6+} complex ions.

$$(NH_4)_7Mo_7O_{24} + CA \rightarrow [Mo - CA]^{6+} \quad (1)$$

Further, Mo^{6+} complex ions have been reduces to Mo^{4+} ions by using sodium borohydrate.

$$[Mo - CA]^{6+} + NaBH_4 \rightarrow Mo^{4+} + CA + NaH + BH_3 \quad (2)$$

Sodium tellurite decomposes through $2Na^+$ and TeO_3^{2-}.

$$Na_2TeO_3 \rightarrow 2Na^+ + TeO_3^{2-} \quad (3)$$

The addition of sodium borohydrate yields pure tellurium and further decomposes to Te^{2-} ions

$$2TeO_3^{2-} + NaBH_4 \rightarrow 2Te + BH_3 + NaH + 3O_2 \quad (4)$$

$$2Te + NaBH_4 \rightarrow 2Te^{2-} + NaH + BH_3 \quad (5)$$

The successive immersion of substrates in the separate precursors containing Mo^{4+} and Te^{2-} ions produces visible, uniform and well adherent $MoTe_2$ thin layer over the substrates by using the following reaction kinetics

$$Mo^{4+} + 2Te^{2-} \rightarrow MoTe_2 \quad (6)$$

Structural study

Figure 1 (a) illustrates comparative structural patterns of prepared SS/$MoTe_2$, SS/MWCNTs and SS/MWCNTs/$MoTe_2$ thin films with stainless steel (SS) as a reference. The most prominent peak observed at 35.17º for $MoTe_2$ and composite thin films is in good agreement with the hexagonal phase of crystalline $MoTe_2$ (JCPDS card no. 73-1650). The other (004), (101) and (107) planes corresponding to 2θ values at 25.48, 29.98 and 54.94º, respectively follows prominent hexagonal phase of $MoTe_2$. The clear and well defined peak obtained at 27.07º for MWCNTs and composite films corresponds to graphitic carbon from MWCNTs, confirming the formation of composite. Liu et al have reported ultrathin nanosheets of few layered $MoTe_2$ thin film which shows hexagonal crystal structure towards significant electrochemical properties[13]. The electrochemically deposited hexagonal $MoTe_2$ film with nanodendrites surface morphology has been successfully utilized for electocatalytic hydrogen evolution[18]. Also, Ding et al. have fabricated vertically stacked hexagonal p-$MoTe_2$ over n-MoS_2 heterostructures by using a single-run chemical vapor deposition (CVD) method for an efficient optoelectronic device as photodetector[19]. Raman spectroscopy measurement is the trustworthy analytic tool in order to confirm the material formation. Figure 1 (b) exhibits the relative Raman spectrum of MWCNTs and MWCNTs/$MoTe_2$ composite. The peaks obtained at low-wave number such as 112, 126, 161, and 167 cm^{-1} (Inset of Figure 1 (b)) are associated with A_g modes of the hexagonal $MoTe_2$, whereas the isolated peak at 189 cm^{-1} is attributed to the B_g mode of the hexagonal $MoTe_2$[13, 16, 20, 21]. Contrary, at high wave number

region, three major peaks obtained at 1350, 1580, and 2712 cm^{-1} are associated with disorderly induced D, G, and 2D bands of graphitic MWCNTs[22]. Furthermore, the peak intensity of all three D, G, and 2D bands of composite sample has been observed to be enhanced compared to bare MWCNTs due to the local electromagnetic field affected SERS (surface enhanced Raman scattering) for the presence of nanostructured $MoTe_2$[22, 23]. Shi et al.[24] have reported amorphous phase of $MoTe_2$ thin film at room temperature by magnetron co-sputtering where prominent Raman mode of A_{1g} with corresponding hexagonal crystal structure was observed due to the annealing effect. Also, large area sputtered CVD deposited $MoTe_2$ thin film shows A_g and B_g Raman modes and effectively utilized as high performance counter electrode for dye-sensitized solar cell[25].

The valence states and surface chemical composition of MWCNTs/$MoTe_2$ can be analysed by using XPS study. The XPS survey spectrum specifies the co-existence of molybdenum (Mo) and tellurium (Te) elements with a contribution of carbon (C) in the composite sample (Figure 1c). A core level spectrum of each element is given in Figure 1(d-f). The peaks at 284.7, 287.3 and 289.1 eV are assigned to C 1s, implying the presence of adventitious carbon and sp^3 hybridized graphitic carbon in MWCNTs along with hydrocarbonate due oxygenated functional groups (Figure 1d)[26]. The binding energy at 234.2 and 237.3 eV were assigned to the Mo $3d_{5/2}$ and Mo $3d_{3/2}$, respectively (Figure 1e)[27, 28]. In Figure 1f, the peaks at 577.9 and 588.3 eV corresponds to the Te $3d_{5/2}$ and Te $3d_{3/2}$, respectively[13, 18, 28]. The spectrum of Mo 3d and Te 3d indicates that Mo and Te exist in +4 and -2 oxidation states, respectively which are the pre-requisite condition to form $MoTe_2$ compound. Xie et al. have obtained these dominant peaks for fast solid-phase synthesized $MoTe_2$ thin film[29].

Surface morphology

Thin film growth with nano surface architecture plays vital role to quantify the utility of thin film electrode towards the supercapacitor application. In this regards, figure 2 (a-d) shows the field emission-scanning electron microscopy (FE-SEM) images of MWCNTs, $MoTe_2$, and MWCNTs/$MoTe_2$ thin film electrodes, respectively. Figure 2 (a) depicts the porous network like surface architecture of MWCNTs which facilitates high surface area, excellent chemical stability and mechanical flexibility. Figure 2 (b) illustrates the FE-SEM image of $MoTe_2$ thin film onto SS substrate. It reveals the nanopebbles like structure close to spherical shape with non-uniform growth leading to porous structure which may boosts the electrochemical access for electrolyte interaction during charge-discharge. Figure 2 (c, d) exhibits FE-SEM images of $MoTe_2$ coated MWCNTs composite surface at two different magnifications. It illustrates the mixed growth of MWCNTs and $MoTe_2$ which is quite supportive sign of interfacial conjugation and synergy between both nanostructures. In literature, such ingrained morphology have been obtained for MWCNTs hybrid materials and utilized for supercapacitor application. Salunkhe et al.[30] have reported articulate coaxial growth of $Ni(OH)_2$ over oxidized CNTs for supercapacitor application. Impressively, Gopi et al.[31] have reported mixed growth of CNT/PbS, CNT/NiS, CNT/CuS, and CNT/CoS composites over Ni-foam substrate for effective use in solar cell and supercapacitor. The EDS and elemental pattern of SS/MWCNTs/$MoTe_2$ composite sample is shown in Figure 2 (e). Inset of Figure 2e shows atomic percentage of 50.81, 11.76 and 37.43% for C, Mo and Te elements, respectively in the composite sample. Figure 2 (f) depicts selected area elemental mapping images of C, Mo and Te elements, respectively. It reveals nearly stoichiometric density ratio of the constituent elements implying the existence of C, Mo and Te elements in composite sample. Tellurium based compound of NiTe shows nearly atomic percentage ratio of about 1:1 for Ni and Te elements[32]. Similarly, for molybdenum based compound of MoS_2

exhibits nearly predicted atomic percentage ratio of about 1:2 for Mo and S elements, respectively[33].

Figure 3 (a) illustrates the TEM analysis of MWCNTs/$MoTe_2$ composite sample. It reveals the dominance of $MoTe_2$ and MWCNTs as mixed growth where it clearly exhibits anchoring of $MoTe_2$ nanopebbles on MWCNTs network. Refluxing MWCNTs with H_2O_2 generate oxygenated functional groups which act as an active site to attach $MoTe_2$ nanopebbles to form nanocomposite. Figure 3 (b) illustrates the HRTEM image of MWCNTs/$MoTe_2$ sample. Figure 3 (c, d) clearly depict the lattice fringes with interplanar spacing of 0.29 nm and 0.35 nm corresponding to (002) plane of characteristic graphitic MWCNTs and prominent (103) plane of hexagonal $MoTe_2$, respectively. Selected area electron diffraction (SAED) pattern shows concentric rings, suggesting polycrystalline nature of the composite sample[34]. The observed planes matches well with the structural results confirming strong evidence for the formation of MWCNTs/$MoTe_2$ composite.

Supercapacitor study

The conventional three electrode electrochemical system was employed to explore the potential application of MWCNTs, $MoTe_2$ and MWCNTs/$MoTe_2$ thin films as supercapacitive electrodes. The $MoTe_2$ electrode was tested in different electrolytes and electrolyte concentrations to obtain the better electrochemical performance and to study the nature of charge-storage (Supporting Information, S3). The 1M NaOH was elevated electrolyte to study the further electrochemical analysis. The comparative electrochemical performance was studied through cyclic voltammetry (CV) analysis at constant scan rate of 100 mV/s for all three electrodes, respectively (Figure 4 (a)). It is observed that, the SS/MWCNTs electrode shows rectangular CV shape with lower current distribution, implying ideal electric double layer capacitive behavior whereas SS/$MoTe_2$ electrode exhibits

faradaic (pseudocapacitive) charge storage with well resolved oxidation and reduction peaks in NaOH electrolyte. The possible electrochemical reaction kinetics can be depicted as follows:

$$MoTe_2 + OH^- \leftrightarrow MoTe_2OH + e^- \quad (7)$$

Generally, the aqueous electrolytes can be categorized into three parts viz.: acidic, alkaline and neutral[17, 22, 35]. The electrode-electrolyte interaction with suitable charge storage mechanism (faradaic or non-faradaic) plays a crucial role for the better electrode performance. The faradaic charge storage mechanism is based on either intercalation or redox reaction. According to literature, alkaline electrolytes always show redox reaction with clearly distinguishable reduction and oxidation peaks due to OH^- ions[35]. In reaction predicted above, Na^+ acts as counterions which never take part in the electrochemical reaction in three electrode system[36]. Similar reports are available for Bi_2S_3:PbS, CoS, SnS and $ZnFe_2O_4$ electrodes where OH^- ions working in negative potentials region[37-40].

We believe the composite electrode shows enhancement in current distribution with nearly rectangular CV shape along with two well distinguished oxidation and reduction peaks; suggesting synergic effect of both the MWCNTs and $MoTe_2$ materials exhibiting materials mutualism. Further, the CV was performed for composite electrode at different scan rate ranging from 2 to 100 mV/s and depicted in Figure 4 (b) (Supporting Information, S4 for SS/MWCNTs and SS/$MoTe_2$). The proportional current distribution and sustained CV shape with respect to increase in the scan rate is the indication of the capacitive behavior and good rate capability of mixed nanostructured growth. The charge storage mechanism is both capacitive and diffusion type as seen by the shape of CV curves. The total charge (q_t) stored by electrode is the addition of the surface charge (q_s) and diffusion controlled charge (q_d) as follows:

$$q_t = q_s + q_d \quad (8)$$

The 'q_s' is the charge generated at electrode-electrolyte interface and have fast charge-discharge whereas 'q_d' charge is due to faradic redox reaction within the bulk and possess slower kinetics compared to 'q_s'. Semi-infinite linear diffusion is supposed for the diffusion processes of 'q_d' and thus, 'q_d' varies as the reciprocal square root of scan rate[41]. The outer charge, 'q_s' should not depend on scan rate[42]. CV measurements can be used to scrutinize these two charge constituents by calculating the dependence of the scan rate and on total charge contribution (q_t)[43],

$$q_t = q_s + k\nu^{-1/2} \quad (9)$$

where, 'k' is a constant and 'υ' is a scan rate. Thus, the total charge (q_t) can be assessed by assuming 'ν' goes to infinity in the plot of specific charge 'q' versus '$\nu^{1/2}$' (Figure 4 (c)). On the other hand, 'q_s' can be evaluated by assuming 'ν' tends to infinity in the plot of '1/q' versus '$\nu^{-1/2}$' (Figure 4 (d)). The discrepancy in the linearity at maximum scan rate is due to the polarization effect which is overlooked from the above equation. The plot of the total specific charge by isolating 'q_s' and 'q_d' at various scan rates is depicted in Figure 4 (e). Excitingly, the evaluated results of surface capacitive (38 %) and diffusion controlled charges (62 %) at low scan rate (2 mV/s) are strongly suggests the faradaic nature of SS/MWCNTs/$MoTe_2$ hybrid electrode during the charge-discharge process. The charge storage contribution of composite electrode at various scan rates is tabulated in detail (Table S1, Supporting Information, S5). Figure 4 (f) shows the specific capacitance values at different scan rate ranging from 2 to 100 mV/s for MWCNTs, $MoTe_2$ and MWCNTs/$MoTe_2$ electrodes, respectively. The dominating specific capacitance of 502 F/g was obtained for composite electrode as compared to the individual $MoTe_2$ (243 F/g) and MWCNTs (102 F/g). The value of specific capacitance has been diminished at higher scan rate for all three

electrodes. This is because, at low scan rate, the effective active sites and pores of material can be maximum utilized by the electrolyte ions whereas at high scan rate, the effective material utilization is limited due to time constraint. Table 1 shows the comparative literature data of composite electrodes[44-49]. Galvanostatic charge-discharge (GCD) is another technique to study the supercapacitor behavior of the electrode materials (Supporting Information, S6).

Electrochemical stability is an important tool to evaluate the material towards energy storage application. The redox active material does not show bearable stability like typical electric double layer materials due to the degradation of active material during each oxidation and reduction process. Figure 5 (a) shows the CV curves for SS/MWCNTs/$MoTe_2$ composite at the fixed scan rate of 100 mV/s. The reduction in area under the CV curves with existence of oxidation and reduction peaks even at 5000 cycles is a good sign of reversibility. Figure 5 (b) shows the retention plot of composite electrode with respect to cycles which depicts the linear decrement in capacity retention with increase in cycles and attained 81% at 5000 cycles. Appearance of such extraordinary retention might be due to synergic effect and effective materials mutualism between MWCNTs and $MoTe_2$. The morphological and elemental perturbation after 5000 number of CV cycles of composite sample was examined by FESEM and EDS analysis (Figure 5 (c and d)). It clearly shows insignificant degradation of the active material even at 5000 CV cycles. The comparative stability studies of MWCNTs, $MoTe_2$ and MWCNTs/$MoTe_2$ is discussed in detail (Supporting Information, S7).

Flexible complete solid-state symmetric supercapacitor (FCSS-SC) device

Formed SS/MWCNTs/$MoTe_2$ composite electrode properties can be well utilized for the fabrication of flexible complete solid-state symmetric supercapacitor (FCSS-SC) device. In this regard, two composite electrodes of same dimensions were sandwiched by implanting PVA-$LiClO_4$ as gel electrolyte. The PVA-$LiClO_4$ gel electrolyte preparation and fabrication

of FCSS-SC device is discussed in detail in Supporting Information, S8. The obvious wide working potential was expected to be benefited to increase the energy density of the device; hence prepared FCSS-SC device was tested at different working potential range at constant scan rate of 100 mV/s (Figure 6 (a)). The FCSS-SC device exhibited 1.4 V working potential range without altering the symmetry of positive and negative current under CV curves. Further, the CV analysis was performed at different scan rates (5 to 100 mV/s) under the potential limit of 1.4 V (Figure 6 (b)) where no perturbation was detected, implying excellent capacitive properties and high rate capability. In order to compare the performance of symmetric solid-state devices, the individual devices based on SS/MWCNTs, SS/$MoTe_2$ and SS/MWCNTs/$MoTe_2$ electrodes were fabricated by using PVA-$LiClO_4$ gel electrolyte (Supporting Information, S9). The performance of the devices were performed by using CV measurements at fixed potential of 1.4 V and constant scan rate of 100 mV/s (Figure S6(a)). Figure S6(b) shows corresponding specific and areal capacitance values with respective device configurations and detail explanation therein. Figure 6 (c) shows the GCD curves collected at different current densities (0.2 to 1 mA/cm^2), where nearly triangular shapes with very small IR drop is observed due to the internal resistance of the material; implying FCSS-SC device follows pseudocapacitive intercalation/deintercalation reaction mechanism during charge storage.

$$MoTe_2 + Li^+ + e^- \leftrightarrow Li - MoTe_2 \qquad (10)$$

The specific capacitances deliberate from the integral area of GCD curves at different current densities are shown in figure 6 (d).

Moreover, the energy and power densities of FCSS-SC device were determined from GCD parameters and illustrated as a Ragone plot (Figure 7 (a)). The supercapacitive parameters associated with FCSS-SC device are summarized in Table 2. According to

previous literature of symmetric and asymmetric devices based on PVA-$LiClO_4$ gel electrolyte possess moderate energy densities such as V_2O_5/CNT (72 Wh/kg)[50], CuS (12 Wh/kg)[51], MnO_2//SnS (29.8 Wh/kg)[39], VS_2/MWCNTs (42 Wh/kg)[22], FeS (2.56 Wh/kg)[34], MnO_2//Fe_2O_3 (41.8 Wh/kg)[52] and MoS_2/MWCNTs (7.90 Wh/kg)[53]. Apart from PVA-$LiClO_4$ gel electrolyte, other symmetric and asymmetric devices have been emerged such as rGO-PMo_{12} (17.20 Wh/kg)[54], $FeCo_2O_4$//AC (24 Wh/kg)[55], MWCNT (2.2 Wh/kg)[56] and activated CNT//MnO_2-graphene (5 Wh/kg)[57]. Some of the other devices are also compared with present FCSS-SC device and associated parameters are summarized in Table 3[34, 53, 54, 58-65]. The siloxene, phosphorene and MXene are such novel materials growing into the demand due to their wide working potential ability with organic electrolytes which further leads to increase energy density of the supercapacitor device[63-65]. Although, obtained FCSS-SC device shows lower energy density value as compared to some literature values, but it promises simple, low-cost, room temperature, more efficient and environmental friendly approach for the synthesis of hybrid thin film and the fabrication of solid-state supercapacitive device. Also this report presents a first attempt not only to synthesize $MoTe_2$ by using SILAR method but also its use to form complete solid-state device.

The recent portable and bendable technological development need light weight and flexible energy storage devices. Hence, bending effect on device performance has been evaluated with bending step of 45° through GCD analysis at constant current density of 0.5 mA/cm^2 (inset of Figure 7 (b)). Insignificant change in the GCD shape even at 175° has been observed implying outstanding mechanical stability of the device with excellent adhesion of the material. Figure 7 (b) exhibits the retention plot with respect to bending angle which shows the reliable elevation in retention after bending the device due to high mechanical strength between substrate and MWCNTs along with nanostructured MWCNTs/$MoTe_2$ hybrid thin film. To explore the commercial usability, the cyclic stability of FCSS-SC device

was tested upto 2000 CV cycles at fixed scan rate of 100 mV/s within optimized potential window of 1.4 V (Inset of Figure 7 (c)), where, insignificant change was observed even at 2000 CV cycles. Figure 7c shows the plot of retention with the CV cycles. Interestingly, the FCSS-SC device exhibits only 6% reduction in its initial value; implying excellent future scope of formed FCSS-SC device as energy storage. The real demonstration of symmetric FCSS-SC device is performed by glowing light emitting diode (LED) (Figure 7 (d)). The device was charged with 3 V dc supply for 30 s and discharge through the red LED. Interestingly, the LED glows upto 60 s; suggesting symmetric FCSS-SC device has better charge storing capability with significant energy and power density.

Electrochemical impedance spectroscopy (EIS) is an important tool to scrutinize the resistive and capacitive components allied with designed electrodes. Figure 8 (a) illustrates Nyquist plot of the formed device in the frequency range of 100 mHz to 100 kHz at zero potential and 10 mV AC amplitude. It clearly exhibits the non-zero intercept on real axis analogous to solution resistance (R_s) which includes contact resistance between electrode and current collector, ionic resistance of gel electrolyte and intrinsic resistance of active electrode[66]. Further, the sequential semicircular arc signifies charge transfer resistance (R_{ct}) due to the presence of reversible faradic reaction during charge-discharge[67]. The values of R_s and R_{ct} are 3.01 and 18.97 Ω, respectively. Such low value of R_s and R_{ct} not only propose better access for electron transfer during charge-discharge but also indicates significant scope towards commercial fabrication. Figure 8 (b) depicts the corresponding equivalent circuit components starts consuming with R_s, whereas R_{ct} and C_{dl} (double layer capacitance) are in parallel arrangement to describe the notable arc. Further, consecutive parallel combination of constant phase element (CPE) and leakage resistance (R_L) are due to the non-uniform distribution of charges[34]. In CPE, 'Y_o' is an admittance and 'n' is an exponential. The straight line nearly parallel to imaginary axis is represented by Warburg resistance (W) which is due

to the diffusion of electrolyte ions[50]. Table 4 depicts obtained values of associated parameters from equivalent circuit analysis.

Figure 8 (c) shows Bode plot in the frame of phase angle and frequency. At low frequency state, the phase angle increases to -74º which tends towards -90º approves capacitive behavior of symmetric FCSS-SC device[68]. Moreover, the frequency at which the phase angle crosses 45° angle is proposed as an ideal capacitive and resistive characteristic[22]. In this concern, the relaxation time constant (t_o) is a valuable tool in order to scrutinize their applicability. The poor value of t_o imply high power delivery which is a concern of basic capacitive feature. The t_o (155 ms) was intended using the relation $t_o = \frac{1}{f_o}$ in which f_o is a characteristic frequency marks at -45º phase angle[69]. The electrochemical activity of supercapacitor device can also be evaluated by figuring real (C') and imaginary (C") capacitances with respect to frequency[22, 23] as follows:

$$C(\omega) = C'(\omega) - jC"(\omega) \quad (11)$$

where,

$$C'(\omega) = \frac{Zim(\omega)}{|Z(\omega)|^2\omega} \quad (12)$$

$$C"(\omega) = \frac{Zr(\omega)}{|Z(\omega)|^2\omega} \quad (13)$$

where 'Z' is the complex impedance represented as '$Z(\omega) = Zr(\omega) + Zim(\omega)$' and '$\omega$= 2πf' with 'f' is the frequency. 'C'(ω)' is the definite approachable capacitance of the electrode whereas 'C"(ω)' is the energy deprivation due to the irreversible routes of the electrodes. On the other hand, 'Zr' and 'Zim' are the real and imaginary parts of the impedance in the Nyquist plot, respectively. Figure 8 (d) shows the plot of real and imaginary capacitances (C' and C") with respect to the frequency. The maximum capacitance is

perceived at lower frequency as the capacitor works as an open circuit at lower frequency while it acts as a short circuit as the frequency tends to infinity[70]. Subsequently, the value of capacitance falls with increase in frequency. Generally, more time is essential to charge-discharge process for low frequency supercapacitors, therefore all the active electrode material exploitation takes place during charge storage. On the other side, less time required for charge-discharge for high frequency supercapacitors but results in lower capacitance. The imaginary capacitance frequency projection goes through a maximum at a specific frequency of 5.35 Hz (t_0 = 186 ms) which implies that the least time required to discharge entire energy from the device (t_0), which is nearly identical as compared to the value obtained from the Bode plot.

Conclusions

In abridgment, a facile, inexpensive, environmental friendly 'dip and dry' followed by successive ionic layer adsorption and reaction (SILAR) methods were explored successfully to get complex conjugate of MWCNTs and $MoTe_2$ in the thin film form. Present investigation is the first report to form SS/MWCNTs/$MoTe_2$ comosite through chemical route with enhanced supercapacitive performance obtained through materials mutualism. In three electrode configuration, the composite electrode exhibited superior specific capacitance of 502 F/g at 2 mV/s scan rate with maximum contribution from diffusion controlled charge. This novel approach have also been proved through flexible complete solid-state symmetric supercapacitive (FCSS-SC) device which showed better specific capacitance, significant energy density and improved electrochemical stability as well. We strongly believe that the projected work on materials mutualism and their effect on supercapacitive enhancement open up the progressive way towards raising the energy storage capability.

ASSOCIATED CONTENT

Supporting Information

Deposition of MWCNTs; Characterizations; Effect of different electrolytes; Concentration variation; CV curves in various electrolytes for $MoTe_2$ electrode; Specific capacitance value for various electrolytes; Effect of NaOH concentration on CV curves; Specific capacitance with different concentrations of NaOH electrolyte; CV curves for SS/MWCNTs and SS/$MoTe_2$ electrodes different scan rates; Contribution of surface adsorbed and diffusion controlled charges; Comparative GCD curves for SS/MWCNTs, SS/$MoTe_2$ and SS/MWNTs/$MoTe_2$ electrodes; GCD plot for SS/MWNTs/$MoTe_2$ electrode at different current densities; Specific capacitance values with respect to current densities; CV curves for SS/MWCNTs, SS/$MoTe_2$ and SS/MWCNTs/$MoTe_2$ electrodes for different cycle number; Capacity retention with number of cycles; Specific and areal capacitance values associated with different device configuration; CV curves of different device configurations of SS/MWCNTs, SS/$MoTe_2$ and SS/MWNTs/$MoTe_2$; Specific and areal capacitance values of different device configuration.

Acknowledgment

Authors acknowledges to DST/TMD/MES/2k16/09 project, Government of India.

References

(1) Xu, M.; Liang, T.; Shi, M.; Chen, H. Graphene-Like Two-Dimensional Materials. *Chem. Rev.*, **2013**, 113, 3766-3798. **DOI**: 10.1021/cr300263a.

(2) Butler, S. Z.; Hollen, S. M.; Cao, L.; Cui, Y.; Gupta, J. A.; Gutierrez, H. R.; Heinz, T. F.; Hong, S. S.; Huang J.; Ismach, A. F.; Johnston-Halperin, E.; Kuno, M.; Plashnitsa, V. V.; Robinson, R. D.; Ruoff, R. S.; Salahuddin, S.; Shan, J.; Shi, L.; Spencer, M. G.; Terrones,

M.; Windl, W.; Goldberger. J. E. Progress, Challenges, and Opportunities in Two-Dimensional Materials Beyond Graphene. *ACS Nano,* **2013**, 7, 2898-2926. **DOI**: 10.1021/nn400280c.

(3) Chhowalla, M.; Shin, H. S.; Eda, G.; Li, L. J.; Loh, K. P.; Zhang, H. The chemistry of two-dimensional layered transition metal dichalcogenide nanosheets. *Nat. chem.*, **2013,** 5, 263-275. **DOI**: 10.1038/nchem.1589.

(4) Mane, R. S.; Sankapal, B. R.; Lokhande C. D. A chemical method for the deposition of Bi_2S_3 thin films from a non-aqueous bath. *Thin Solid Film*, **2000**, 359, 136-140. **DOI:** 10.1016/S0040-6090(99)00532-5.

(5) Sankapal, B. R.; Lokhande, C. D. Effect of annealing on chemically deposited Bi_2Se_3-Sb_2Se_3 composite thin films. *Mater. Chem. Phy.*, **2002**, 74, 126-133. **DOI:** 10.1016/S0254-0584(01)00414-X.

(6) Ahire, R. R.; Sankapal, B. R.; Lokhande, C. D. Photoelectrochemical characterization of chemically deposited $(CdS)_x(Bi_2S_3)_{1-x}$ composite thin films. *Mater. Chem. Phy.*, **2001**, 72, 48-55. **DOI:** 10.1016/S0254-0584(01)00311-X.

(7) Zhang, C.; Yin, H.; Han, M.; Dai, Z.; Pang, H.; Zheng, Y.; Lan, Y. Q.; Bao, J.; Zhu, J. Two-Dimensional Tin Selenide Nanostructures for Flexible All-Solid-State Supercapacitors. *ACS Nano*, **2014**, 8, 3761-3770. **DOI**: 10.1021/nn5004315.

(8) Zhang, Y.; Pan, A.; Wang, Y.; Cao, X.; Zhou, Z.; Zhu, T.; Liang, S.; Cao, G. Self-templated synthesis of N-doped $CoSe_2$/C double-shelled dodecahedra for high-performance supercapacitors. *Energy Storage Materials*, **2017** 8, 28-34. **DOI**: 10.1016/j.ensm.2017.03.005.

(9) Tang, C.; Pu, Z.; Liu, Q.; Asiri, A. M.; Sun, X.; Luo, Y.; He, Y. In Situ Growth of NiSe Nanowire Film on Nickel Foam as an Electrode for High-Performance Supercapacitors. *ChemElectroChem*, **2015**, 2, 1903-1907. **DOI**: 10.1002/celc.201500285.

(10) Xia, C.; Jiang, Q.; Zhao, C.; Beaujuge, P. M.; Alshareef, H. N. Asymmetric supercapacitors with metal-like ternary selenides and porous graphene electrodes. *Nano Energy*, **2016,** 24, 78-86. **DOI**: 10.1016/j.nanoen.2016.04.012

(11) Javed, M. S.; Dai, S.; Wang, M.; Guo, D.; Chen, L.; Wang, X.; Hu, C.; Xi, Y. High performance solid state flexible supercapacitor based on molybdenum sulfide hierarchical nanospheres. *J. Power Sources*, **2015**, 285, 63-69. **DOI**: 10.1016/j.jpowsour.2015.03.079.

(12) Peng, H.; Wei, C.; Wang, K.; Meng, T.; Ma, G.; Lei, Z.; Gong, X. $Ni_{0.85}Se$@$MoSe_2$ Nanosheet Arrays as the Electrode for High-Performance Supercapacitors. *ACS Applied Materials & Interfaces*, **2017**, 9, 17067-17075. **DOI**: 10.1021/acsami.7b02776.

(13) Liu, M.; Wang, Z.; Liu, J.; Wei, G.; Du, J.; Li, Y.; An, C.; Zhang, J. Synthesis of few-layer 1T′-$MoTe_2$ ultrathin nanosheets for high-performance pseudocapacitors. *J. Mater. Chem. A*, **2017**, 5, 1035-1042. **DOI**: 10.1039/C6TA08206H.

(14) Yang, Y.; Fei, H.; Ruan, G.; Xiang C.; Tour, J. M. Edge-Oriented MoS_2 Nanoporous Films as Flexible Electrodes for Hydrogen Evolution Reactions and Supercapacitor Devices. *Adv. Mater.*, **2014**, 26, 8163-8168. **DOI**: 10.1002/adma.201402847.

(15) Hu, Z.; Wang, L.; Zhang, K.; Wang, J.; Cheng, F.; Tao, Z.; Chen, J. MoS_2 Nanoflowers with Expanded Interlayers as High-Performance Anodes for Sodium-Ion Batteries. *Angew. Chem.*, **2014**, 126, 13008-13012. **DOI**: 10.1002/ange.201407898.

(16) Liu, M.; Wang, X.; Huang, Z.; Guo, P.; Wang, Z. In-situ solution synthesis of graphene supported lamellar 1T'-$MoTe_2$ for enhanced pseudocapacitors. *Mater. Lett.*, **2017**, 206, 229-232. **DOI**: 10.1016/j.matlet.2017.07.033.

(17) Karade, S. S.; Sankapal, B. R. Room temperature PEDOT:PSS encapsulated MWCNTs thin film for electrochemical supercapacitor. *J. Electroanal. Chem.*, **2016**, 771, 80-86. **DOI**: 10.1016/j.jelechem.2016.04.012.

(18) Zhoua, Y.; Jia, L.; Feng, Q.; Wang, T.; Lia, X.; Wang, C., $MoTe_2$ nanodendrites based on Mo doped reduced graphene oxide/polyimide composite film for electrocatalytic hydrogen evolution in neutral solution. *Electrochim. Acta*, **2017**, 229, 121-128. **DOI**: 10.1016/j.electacta.2017.01.147.

(19) Ding, Y.; Zhou, N.; Gan, L.; Yan, X.; Wu, R.; Abidi, I. H.; Waleed, A.; Pan, J.; Ou, X.; Zhang, Q.; Zhuang, M.; Wang, P.; Pan, X.; Fan, Z.; Zhai, T.; Luo, Z.; Stacking-mode Confined Growth of 2H-$MoTe_2$/MoS_2 Bilayer Heterostructures for UV-Vis-IR Photodetectors. *Nano energy*, **2018,** 49, 200-208**. DOI:** 10.1016/j.nanoen.2018.04.055.

(20) Yamamoto, M.; Wang, S. T.; Ni, M.; Lin, Y.-F.; Li, S. -L.; Aikawa, S.; Jian, W.-B.; Ueno, K.; Wakabayashi K.; Tsukagoshi, K. Strong Enhancement of Raman Scattering from a Bulk-Inactive Vibrational Mode in Few-Layer $MoTe_2$. *ACS Nano*, **2014**, 8, 3895-3903. **DOI**: 10.1021/nn5007607.

(21) Pradhan, N. R.; Rhodes, D.; Feng, S.; Xin, Y.; Memaran, S.; Moon, B. H.; Terrones, H.; Terrones M.; Balicas, L. Field-Effect Transistors Based on Few-Layered α-$MoTe_2$. *ACS Nano*, **2014**, 8, 5911-5920. **DOI**: 10.1021/nn501013c.

(22) Pandit, B.; Karade, S. S.; Sankapal, B. R. Hexagonal VS_2 Anchored MWCNTs: First Approach to Design Flexible Solid-State Symmetric Supercapacitor Device. *ACS Appl. Mater. Interfaces*, **2017**, 9, 44880-44891. **DOI**: 10.1021/acsami.7b13908.

(23) Pandit, B.; Dhakate, S. R.; Singh, B. P.; Sankapal, B. R. Free-standing flexible MWCNTs bucky paper: Extremely stable and energy efficient supercapacitive electrode. *Electrochim. Acta*, **2017**, 249, 395-403. **DOI**: 10.1016/j.eleacta.2017.08.013.

(24) Shi, D.; Wa1ng, G.; Li, C.; Shen, X.; Nie, Q. Preparation and thermoelectric properties of $MoTe_2$ thin films by magnetron co-sputtering. *Vacuum*, **2017,** 138, 101-104. **DOI:** 10.1016/j.vacuum.2017.01.030.

(25) Hussai, S.; Patil, S. A.; Vikraman, D.; Menga, N.; Liu, H.; Song, W.; An, K. S.; Jeong, S. H.; Kim, H. S.; Jung, J. Large area growth of $MoTe_2$ films as high performance counter electrodes for dye-sensitized solar cells. *Sci. Rep.* **2018**, 8, 29 **DOI:** 10.1038/s41598-017-18067-6.

(26) Vidyasagar, D.; Ghugal, S. G.; Kulkarni, A.; Mishra, P.; Shende, A. G.; Jagannath, Umare, S. S.; Sasikala R. Silver/Silver(II) oxide (Ag/AgO) loaded graphitic carbon nitride microspheres: An effective visible light active photocatalyst for degradation of acidic dyes and bacterial inactivation. *Appl. Catal. B Environ.*, **2018**, 221, 339-348. **DOI:** 10.1016/j.apcatb.2017.09.030.

(27) Wang, K.; Yang, J.; Zhu, J.; Li, L.; Liu, Y.; Zhang, C.; Liu T. General solution-processed formation of porous transition-metal oxides on exfoliated molybdenum disulfides for high-performance asymmetric supercapacitors. *J. Mater. Chem. A*, **2017**, 5, 11236-11245. **DOI:** 10.1039/C7TA01457K.

(28) Ouadah, A.; Bernede, J. C.; Pouzet, J.; Morsli, M. MoTe, Thin Films Synthesized by Solid State Reactions between Mo and Te Thin Films. *Phys. Stat. Sol.*, **1992**, 134, 455-466. **DOI:** 10.1002/pssa.2211340215.

(29) Xie, S.; Chen, L.; Zhang, T. B.; Nie, X. R.; Zhu, H.; Ding, S. J.; Sun, Q. Q.; Zhang, D. W. Fast solid-phase synthesis of large-area few-layer 1T'-$MoTe_2$ films. *J. Crystal Growth*, **2017**, 467, 29-33. **DOI:** 10.1016/j.jcrysgro.2017.03.013.

(30) Salunkhe, R. R.; Lin, J.; Malgras, V.; Dou, S. X.; Kim, J. H.; Yamauchi, Y. Large-Scale Synthesis of Coaxial Carbon Nanotube/$Ni(OH)_2$ Composites for Asymmetric Supercapacitor Application. *Nano Energy*, **2015**, 11, 211-218. **DOI**: 10.1016/j.nanoen.2014.09.030.

(31) Gopi, C. V. V. M.; Ravi, S.; Rao, S. S.; Reddy, A. E.; Kim, H. -Jc. Carbon nanotube/metal-sulfide composite flexible electrodes for high-performance quantum dot-sensitized solar cells and supercapacitors. *Sci. Rep.*, **2017**, 17, 46519. **DOI**: 10.1038/srep46519.

(32) Zhou, P.; Fan, L.; Wu, J.; Gong, C.; Zhang, J.; Tu, Y. Facile hydrothermal synthesis of NiTe and its application as positive electrode material for asymmetric supercapacitor. *J. Alloys Comp.* **2016**, 685, 384-390. **DOI:** 10.1016/j.jallcom.2016.05.287.

(33) A. Ramadoss, T. Kim, G. S. Kim, S. J. Kim, Enhanced activity of a hydrothermally synthesized mesoporous MoS_2 nanostructure for high performance supercapacitor applications. *New J. Chem.*, **2014**, 38, 2379-2385. **DOI:** 10.1039/c3nj01558k.

(34) Karade, S. S.; Dwivedi, P.; Majumder, S.; Pandit, B.; Sankapal, B. R. First report on a FeS-based 2 V operating flexible solid-state symmetric supercapacitor device. *Sustainable Energy Fuels*, **2017,** 1, 1366-1375. **DOI**: 10.1039/C7SE00165G.

(35) Zhong, C.; Deng, Y.; Hu, W.; Qiao, J.; Zhang, L.; Zhang J. A review of electrolyte materials and compositions for electrochemical supercapacitors. *Chem. Soc. Rev.*, **2015**, 44, 7484-7539. **DOI:** 10.1039/c5cs00303b

(36) Maheswari, N.; Muralidharan G. Supercapacitor Behaviour of Cerium Oxide Nanoparticles in Neutral Aqueous Electrolytes. *Energy Fuels*, **2015**, 29, 8246-8253. **DOI:** 10.1021/acs.energyfuels.5b02144.

(37) Pandit, B.; Sharma, G. K.; Sankapal, B. R. Chemically deposited Bi_2S_3:PbS solid solution thin film as supercapacitive electrode. *J. Colloid Interface Sci.*, **2017**, 2505, 1011-1017. **DOI**: 10.1016/j.jcis.2017.06.092

(38) Meng, X.; Deng, J.; Zhu, J.; Bi, H.; Kan, E.; Wang, X. Cobalt Sulfide/Graphene Composite Hydrogel as Electrode for High Performance Pseudocapacitors. *Sci. Rep.*, **2016**, 6, 21717. **DOI:** 10.1038/srep21717.

(39) Patil, A. M.; Lokhande, V. C.; Patil, U. M.; Shinde P. A.; Lokhande, C. D. High Performance All-Solid-State Asymmetric Supercapacitor Device Based on 3D Nanospheres of β-MnO_2 and Nanoflowers of O-SnS. *ACS Sustainable Chem. Eng*., **2018**, 6, 787-802. **DOI:** 10.1021/acssuschemeng.7b03136.

(40) Raut, S. S.; Sankapal, B. R. First report on synthesis of $ZnFe_2O_4$ thin film using successive ionic layer adsorption and reaction: Approach towards solid-state symmetric supercapacitor device. *Electrochim. Acta*, **2016**, 198, 203–211. **DOI:** 10.1016/j.electacta.2016.03.059

(41) Ardizzone, S.; Fregonara, G.; Trasatti, S. "Inner" and "outer" active surface of RuO_2 electrodes. *Electrochim. Acta*, ***1990***, 35, 263-267. **DOI**: 10.1016/0013-4686(90)85068-X.

(42) Pétrissans, X.; Bétard, A.; Giaume, D.; Barboux, P.; Dunn, B.; Sicard, L.; Piquemal, J. -Y. Solution synthesis of nanometric layered cobalt oxides for electrochemical applications. *Electrochim. Acta*, **2012**, 66, 306-312. **DOI**: 10.1016/j.electacta.2012.01.104.

(43) Chen, Z.; Augustyn, V.; Jia, X.; Xiao, Q.; Dunn, B.; Lu, Y. High-Performance Sodium-Ion Pseudocapacitors Based on Hierarchically Porous Nanowire Composites. *ACS Nano*, **2012** 6, 4319-4327. **DOI**: 10.1021/nn300920e.

(44) Xiang, D.; Yin, L.; Wang, C.; Zhang L. High electrochemical performance of RuO_2-Fe_2O_3 nanoparticles embedded ordered mesoporous carbon as a supercapacitor electrode material. *Energy*, **2016**, 106, 103-111. **DOI:** 10.1016/j.energy.2016.02.141.

(45) Xiang, D.; Liu, X.; Dong, X. A facile synthetic method and electrochemical performances of nickel oxide/carbon fibers composites. *J Mater Sci.*, **2017**, 52, 7709-7718. **DOI:** 10.1007/s10853-017-1019-4.

(46) Shinde, P. A.; Lokhande, V. C.; Patil, A. M.; Ji, T.; Lokhande C. D. Single-step hydrothermal synthesis of WO_3-MnO_2 composite as an active material for all-solid-state flexible asymmetric supercapacitor. *Inter. J. Hydrogen Energy*, **2017**, 43, 2869-2880 **DOI:** 10.1016/j.ijhydene.2017.12.093.

(47) Chen, M.; Dai, Y.; Wang, J.; Wang, Q.; Wang, Y.; Cheng, X.; Yan, X. Smart combination of three- imensional-flower-like MoS_2 nanospheres/interconnected carbon nanotubes for application in supercapacitor with enhanced electrochemical performance. *J. Alloy Comp.*, **2017**, 696, 900-906. **DOI:** 10.1016/j.jallcom.2016.12.077.

(48) Zhu, T.; Xia, B.; Zhou, L.; Lou, X. W. Arrays of ultrafine CuS nanoneedles supported on a CNT backbone for application in supercapacitors. *J. Mater. Chem.*, **2012**, 22, 7851-7855. **DOI:** 10.1039/c2jm30437f.

(49) Tang, Y.; Chen, T.; Yu, S.; Qiao, Y.; Mu, S.; Hu J.; Gao, F. Synthesis of Graphene Oxide Anchored Porous Manganese Sulfide Nanocrystal via the Nanoscale Kirkendall Effect for supercapacitor. *J. Mater. Chem. A*, **2015**, 3, 12913-12919. **DOI:** 10.1039/C5TA02480C.

(50) Pandit, B.; Dubal, D. P.; Gomez-Romero, P.; Kale, B. B.; Sankapal, B. R. V_2O_5 encapsulated MWCNTs in 2D surface architecture: Complete solid-state bendable highly stabilized energy efficient supercapacitor device. *Sci. Rep.*, **2017**, 7, 43430. **DOI**: 10.1038/srep43430.

(51) Patil, A. M.; Lokhande, A. C.; Chodankar, N. R.; Shinde, P. A.; Kim, J. H.; Lokhande, C. D. Interior design engineering of CuS architecture alteration with rise in reaction bath temperature for high performance symmetric flexible solid state supercapacitor. *J. Ind. Eng. Chem.*, **2017**, 46, 91-102. **DOI**: 10.1016/j.jiec.2016.10.019.

(52) Gund, G. S.; Dubal, D. P.; Chodankar, N. R.; Cho, J. Y.; Gomez-Romero, P.; Park, C.; Lokhande, C. D. Low-cost flexible supercapacitors with high-energy density based on nanostructured MnO_2 and Fe_2O_3 thin films directly fabricated onto stainless steel. *Sci. Rep.*, **2015**, 5, 12454. **DOI**: 10.1038/srep12454.

(53) Karade, S. S.; Dubal, D. P.; Sankapal, B. R. Decoration of Ultrathin MoS_2 Nanoflakes over MWCNTs: Enhanced Supercapacitive Performance through Electrode to Symmetric All-Solid-State Device. *ChemistrySelect*, **2017**, 2, 10405-10412. **DOI**: 10.1002/slct.201701788.

(54) Dubal, D. P.; Suarez-Guevara, J.; Tonti, D.; Enciso, E.; Gomez-Romero, P.; high voltage solid state symmetric supercapacitor based on graphene–

polyoxometalate hybrid electrodes with a hydroquinone doped hybrid gel-electrolyte. *J. Mater. Chem. A*, **2015**, 3, 23483-23492. **DOI**: 10.1039/C5TA05660H.

(55) Tajik, S.; Dubal, D. P.; Gomez-Romero, P.; Yadegari, A.; Rashidi, A.; Nasernejad, B.; Inamuddin.; Asiri, A. M. Nanostructured mixed transition metal oxides for high performance asymmetric supercapacitors: Facile synthetic strategy. *Inter. J. Hydrogen Energy*, **2017**, 42, 12384-12395. **DOI**: 10.1016/j.ijhydene.2017.03.117.

(56) Honda, Y.; Haramoto, T.; Takeshige, M.; Shiozaki, H.; Kitamura, T.; Ishikawa, M. Aligned MWCNT Sheet Electrodes Prepared by Transfer Methodology Providing High-Power Capacitor Performance. *ECS Electrochem. Solid-State Lett.* **2007**, 10, A106-A110. **DOI**: 10.1149/1.2437665.

(57) Xu, L.; Jia, M.; Li, Y.; Jin, X.; Zhang, F. High-performance MnO_2-deposited graphene/activated carbon film electrodes for flexible solid-state supercapacitor. *Sci. Rep.*, **2017**, 7, 12857. **DOI**: 10.1038/s41598-017-11267-0.

(58) Patil, A. M.; Lokhande, A. C.; Chodankar, N. R.; Kumbhar, V. S.; Lokhande, C. D. Engineered morphologies of β-NiS thin films via anionic exchange process and their supercapacitive performance. *Mater. Des.* **2016**, 97, 407-416. **DOI:** 10.1016/j.matdes.2016.02.114.

(59) Chodankar, N. R.; Dubal, D. P.; Gund, G. S.; Lokhande, C. D. A symmetric MnO_2/MnO_2 flexible solid state supercapacitor operating at 1.6 V with aqueous gel electrolyte. *J. Energy Chem.* **2016**, 25, 463-471. **DOI:** 10.1016/j.jechem.2016.01.020

(60) Javed, M. S.; Dai, S.; Wang, M.; Guo, D.; Chen, L.; Wang, X.; Hu, C.; Xi, Y. High performance solid state flexible supercapacitor based on molybdenum sulfide hierarchical nanospheres. *J. Power Sources*, **2015**, 285, 63-69. **DOI:** 10.1016/j.jpowsour.2015.03.079

(61) Karade, S. S.; Sankapal, B. R. Two dimensional cryptomelane like growth of $MoSe_2$ over MWCNTs: Symmetric all-solid-state supercapacitor. *J. Electroanal. Chem.* **2017**, 802, 131-138. **DOI:** 10.1016/j.jelechem.2017.082.017.

(62) Pujari, R. B.; Lokhande, A. C.; Yadav, A.A.; Kim, J. H.; Lokhande C.D. Synthesis of MnS microfibers for high performance flexible supercapacitors. *Mater. Design*, **2016**, 108, 510-517. **DOI:** 10.1016/j.matdes.2016.07.038.

(63) Krishnamoorthy, K.; Pazhamalai, P.; Kim, S. J. Two-dimensional siloxene nanosheets: Novel high-performance supercapacitor electrode materials, *Energy Environ. Sci.*, 2018, 11, 1595-1602. DOI: 10.1039/C8EE00160J.

(64) Xiao, H.; Wu, Z. –S.; Chen, L.; Zhou, F.; Zheng, S.; Ren, W.; Cheng, H. -M.; Bao, X. One-Step Device Fabrication of Phosphorene and Graphene Interdigital Micro-Supercapacitors with High Energy Density. *ACS Nano*, **2017**, 11, 7284-7292. **DOI:** 10.1021/acsnano.7b03288.

(65) Yu, L.; Hu, L.; Anasori, B.; Liu, Y. -T.; Zhu, Q.; Zhang, P.; Gogotsi, Y.; Xu, B. MXene-Bonded Activated Carbon as a Flexible Electrode for High-Performance Supercapacitors. *ACS Energy Lett.* **2018**, 3, 1597–1603. **DOI:** 10.1021/acsenergylett.8b00718.

(66) Dubal, D. P.; Lee, S. H.; Kim, J. G.; Kim, W. B.; Lokhande, C. D. Porous polypyrrole clusters prepared by electropolymerization for a high performance supercapacitor. *J. Mater. Chem.*, **2012**, 22, 3044-3052. **DOI**: 10.1039/C2JM14470K.

(67) Zhou, X.; Wang, Z.; Chen, W.; Ma, L.; Chen, D.; Lee, J. Y. Facile synthesis and electrochemical properties of two dimensional layered MoS_2/graphene composite for reversible lithium storage. *J. Power Sources*, **2014**, 251, 264-268. **DOI**: 10.1016/j.jpowsour.2013.11.060.

(68) Zhang, J.; Zhao, X. S. On the Configuration of Supercapacitors for Maximizing Electrochemical Performance. *ChemSusChem*, **2012**, 5, 818-841. **DOI**: 10.1002/cssc.201100571.

(69) Sheng, K.; Sun, Y.; Li, C.; Yuan W.; Shi, G. Ultrahigh-rate supercapacitors based on eletrochemically reduced graphene oxide for ac line-filtering. *Sci. Rep.*, **2012**, 2, 247. **DOI**: 10.1038/srep00247.

(70) Sivaraman, P.; Kushwaha, R. K.; Shashidhara, K.; Hande, V. R.; Thakur, A. P.; Samui, A. B.; Khandpekar, M. M.; All solid supercapacitor based on polyaniline and crosslinked sulfonated poly[ether ketone]. Electrochim. Acta, 55 (2010) 2451-2456. **DOI**: 10.1016/j.electacta.2009.12.009.

Figures and captions

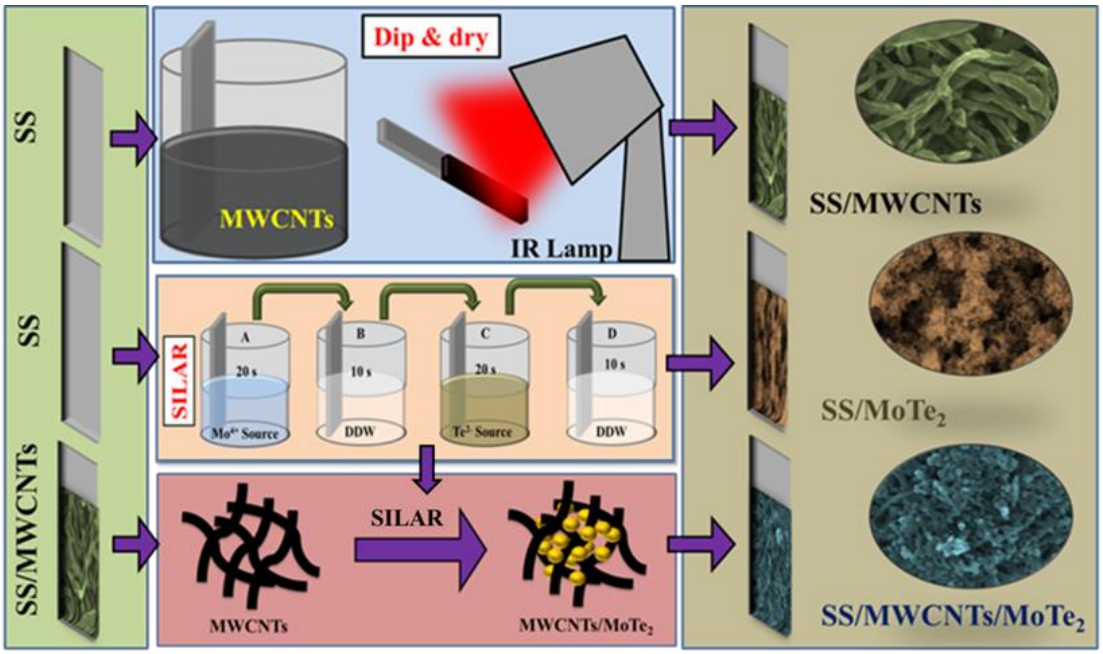

Scheme 1: Schematic presentation of synthesis of SS/MWCNTs, SS/$MoTe_2$ and SS/MWCNTs/$MoTe_2$ composite nanostructured thin films development.

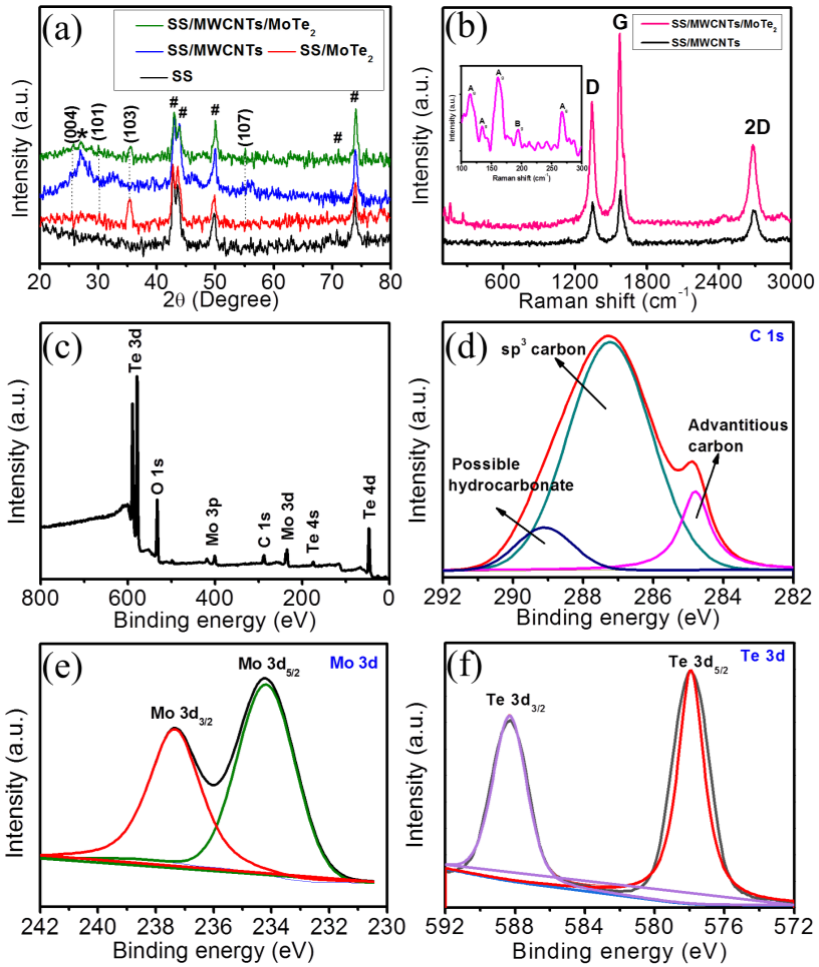

Figure 1: (a) XRD patterns of SS/$MoTe_2$, SS/MWCNTs and SS/MWCNTs/$MoTe_2$ thin films with SS as reference (b) Raman spectra of SS/MWCNTs and SS/MWCNTs/$MoTe_2$ sample, (c) XPS survey spectrum of MWCNTs/$MoTe_2$, Core level XPS spectra for (d) C 1s , (e) Mo 3d and (f) Te 3d, respectively.

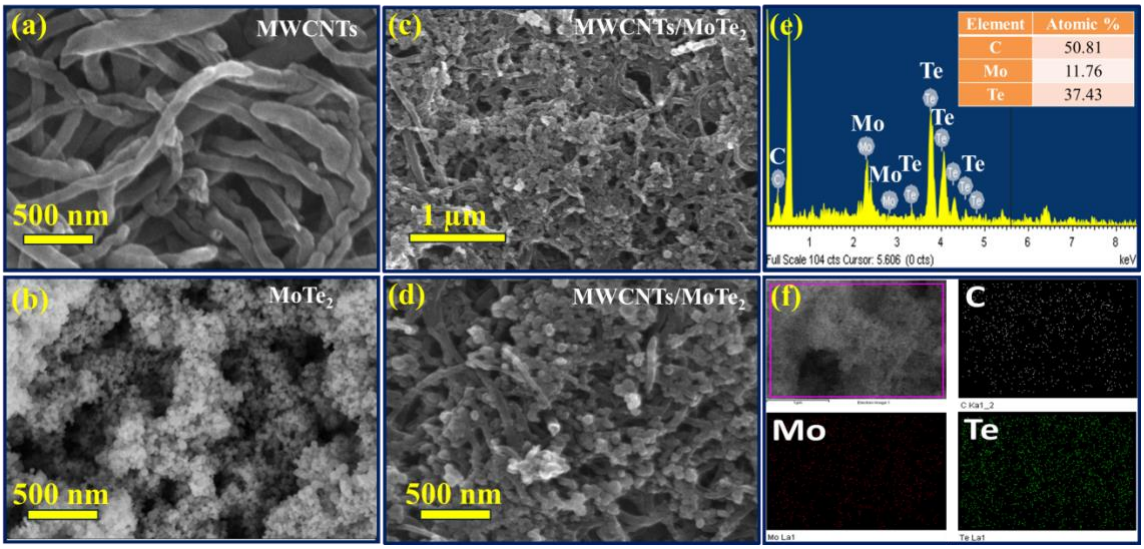

Figure 2: FE-SEM images of (a) SS/MWCNTs, (b) SS/$MoTe_2$, (c & d) SS/MWCNTs/$MoTe_2$, (e) EDS pattern of SS/MWCNTs/$MoTe_2$ sample, inset shows atomic percentage of corresponding elements (f) selected area for elemental mapping and elemental mapping for elements carbon (C), molybdenum (Mo) and tellurium (Te), respectively.

1

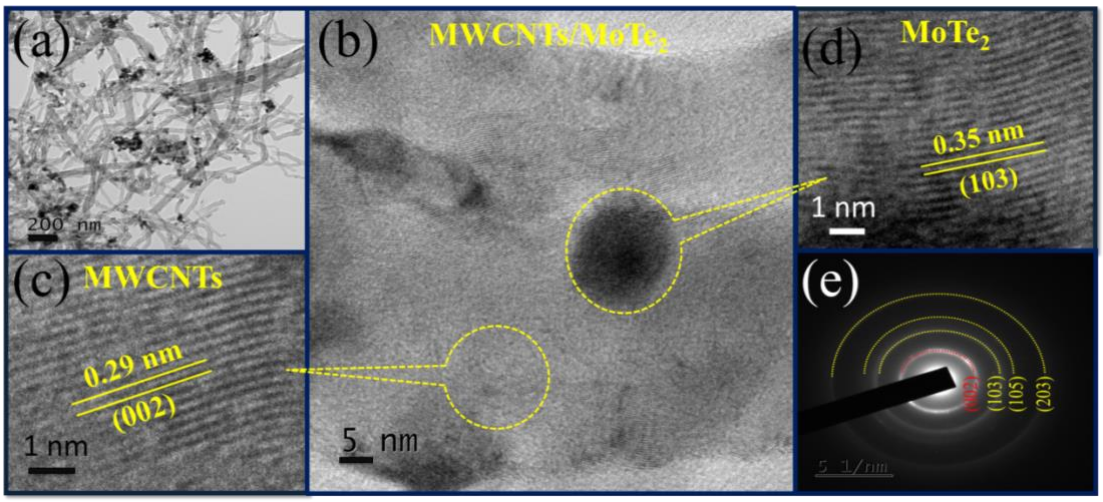

Figure 3: (a) TEM images of MWCNTs/$MoTe_2$ sample (b-d) HR-TEM image of MWCNTs/$MoTe_2$ along with corresponding enlarged views of lattice fringes corresponding to MWCNTs and $MoTe_2$ (e) Corresponding SAED pattern.

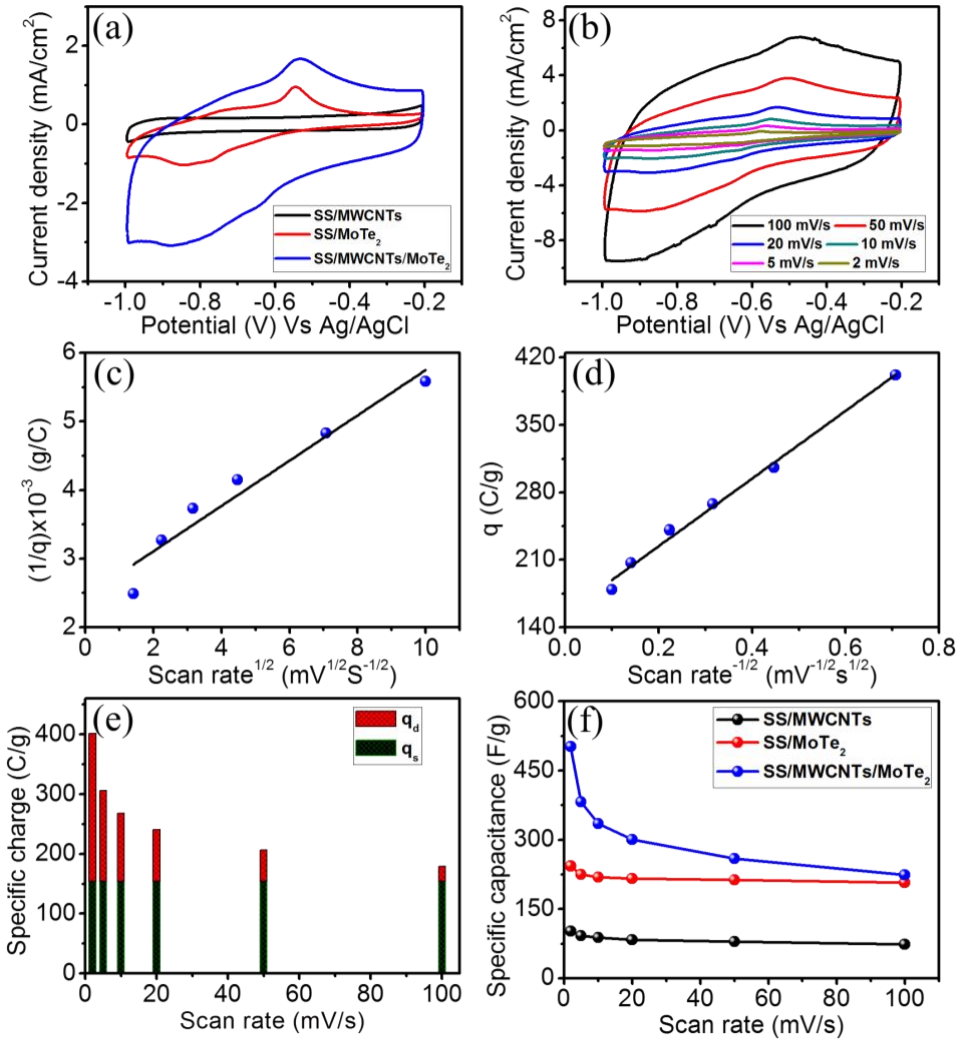

Figure 4: (a) Comparative CV curves of SS/MWCNTs, SS/$MoTe_2$ and SS/MWCNTs/$MoTe_2$ electrodes, (b) CV curves at different scan rates for SS/MWCNTs/$MoTe_2$ composite electrode, (c) Plot of the reciprocal of specific charge (1/q) against the square root of scan rate, (d) Plot of total specific charge (q) against the reciprocal of the square root of potential scan rate, (e) Illustration of the contributions from the surface capacitive (q_s) and diffusion-controlled (q_d) charge to the total charge stored, at different scan rates and (f) Specific capacitance against scan rate for SS/MWCNTs, SS/$MoTe_2$ and SS/MWCNTs/$MoTe_2$ electrodes.

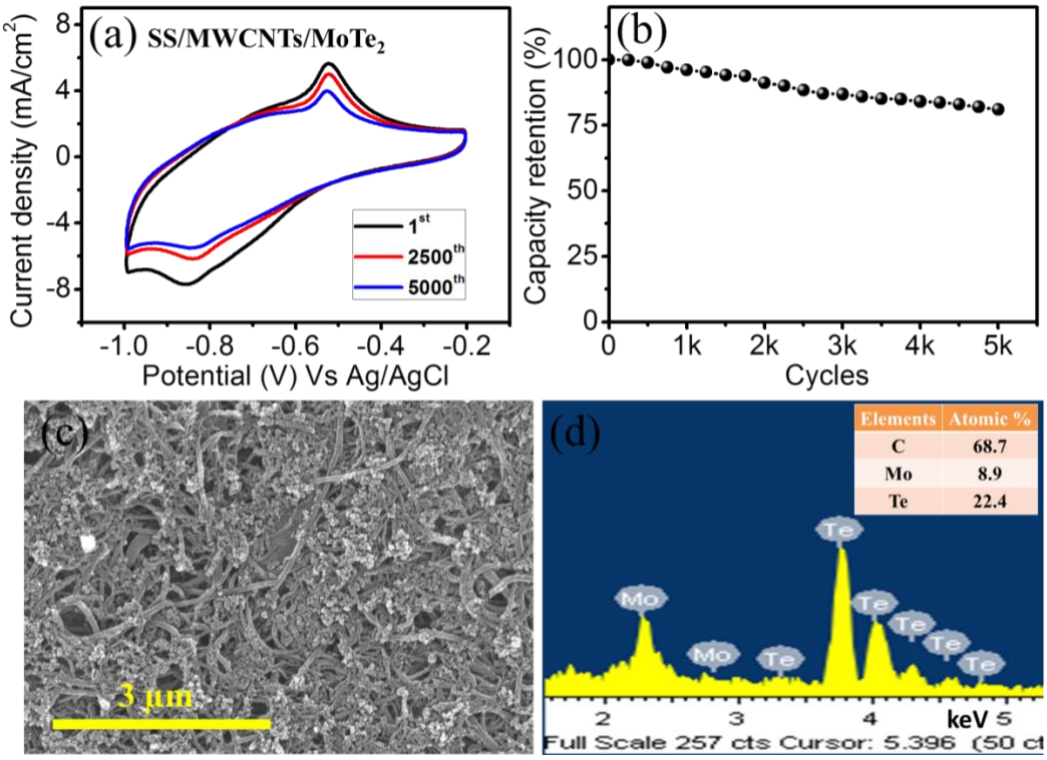

Figure 5: (a) CV curves for SS/MWCNTs/$MoTe_2$ electrodes for different cycle number at 100 mV/s scan rate, (b) Capacity retention with number of cycles for respective electrodes, (c and d) SEM image and EDS pattern of SS/MWCNTs/$MoTe_2$ electrode at 5000 CV cycles.

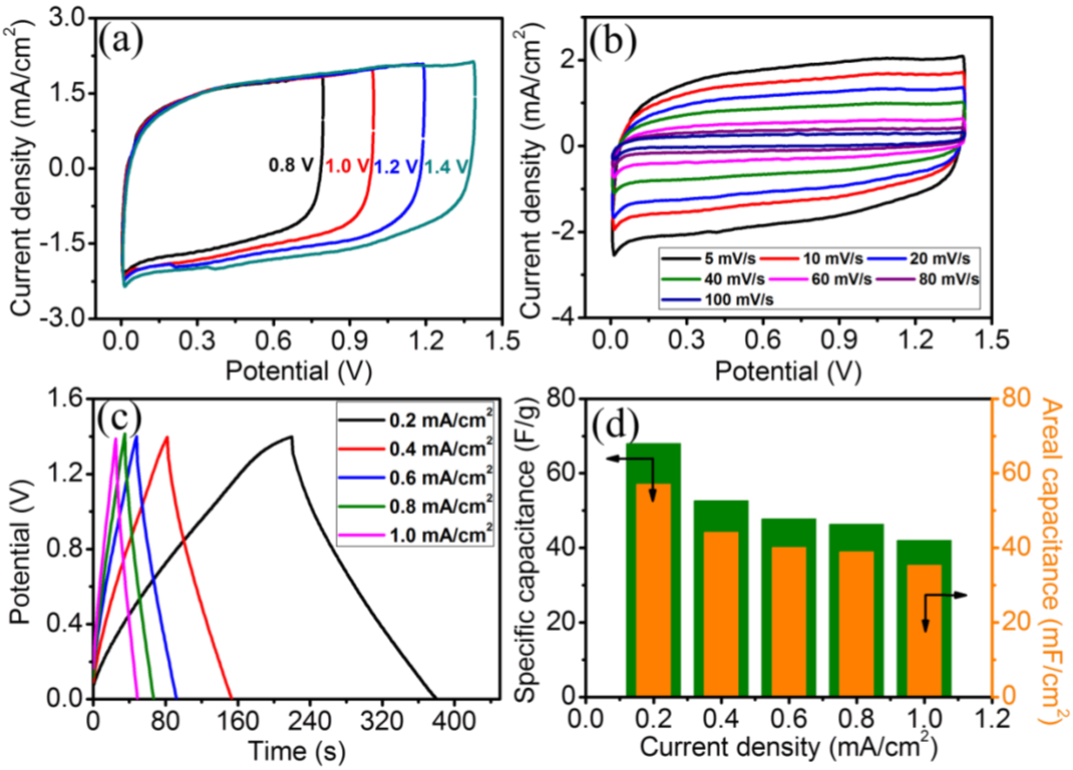

Figure 6: For FCSS-SC device shows (a) CV curves with different potential windows (0.8 to 1.4 V), (b) CV curves at different scan rates (5 to 100 mV/s), (c) GCD curves at different current densities (0.2 to 1 mA/cm^2) and (d) Specific and areal capacitance at different current densities.

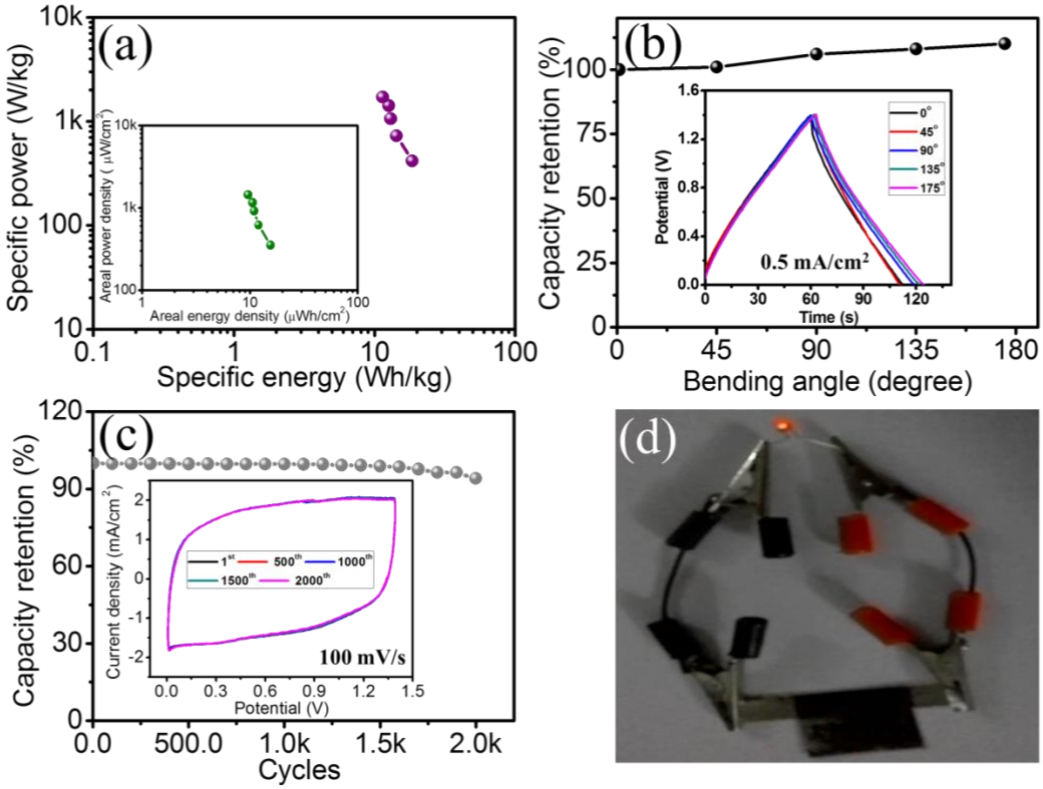

Figure 7 (a) Ragone plot, (b) Plot of capacity retention with bending angle. Inset shows CD curves at different bending angles at 0.5 mA/cm^2 current density, (c) Capacity retention at 2000 cycles. Inset shows CV curves at different cycles at 100 mV/s scan rate, and (d) Actual working of FCSS-SC device to lit up one red LED.

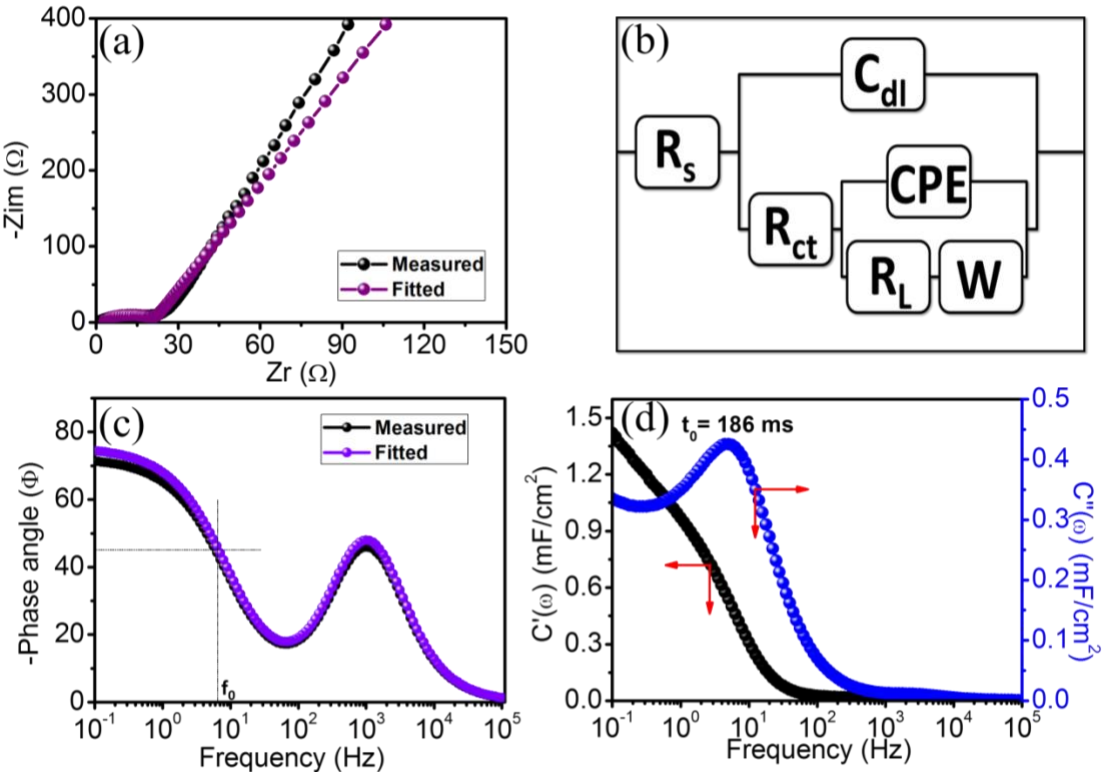

Figure 8 (a) Nyquist plot of imaginary and real part of impedance (b) Corresponding equivalent circuit diagram. (c) Bode plot of phase angle versus frequency and (d) Real and imaginary parts of capacitance (C' and C") versus frequency of FCSS-SC device

Table 1: Comparative supercapacitive performance of composite electrodes.

Material	Method	Electrolyte	Specific capacitance (F/g)	Stability		Ref
				Retention (%)	Cycles	
RuO_2-Fe_2O_3	Impregnation and heating	0.5 M H_2SO_4	1668 at 5 mV/s	93	3000	[44]
NiO/carbon fibre	Electrodeposition	2 M KOH	929 at 5 mV/s	88	5000	[45]
WO_3-MnO_2	Hydrothermal	1 M Na_2SO_4	609 at 5 mV/s	89	2000	[46]
MoS_2/CNT	Hydrothermal	1 M Na_2SO_4	74 at 5 mV/s	81	1000	[47]
CuS/CNT	Chemical conversion	2 M KOH	114 at 5 mV/s	100	1000	[48]
MnS/GO-NH_3	Hydrothermal	2 M KOH	391 at 5 mV/s	81	2000	[49]
MWCNT/$MoTe_2$	SILAR	1 M NaOH	502 at 2 mV/s	81	5000	Present report

Table 2: Specific and areal parameters associated with FCSS-SC device

Current density (mA/cm^2)	Capacitance		Energy density		Power density	
	Specific (F/g)	Areal (mF/cm^2)	Wh/kg	$\mu Wh/cm^2$	W/kg	$\mu W/cm^2$
0.2	68.01	57.12	18.51	15.55	416	352
0.4	52.61	44.19	14.32	12.03	726	618
0.6	47.79	40.14	13.01	10.93	1064	915
0.8	46.31	38.90	12.61	10.59	1418	1155
1.0	42.02	35.29	11.44	9.61	1716	1441

Table 3: The current FCSS-SC device parameters are compared with other literature.

Device	Cell remark	Electrolyte	E (V)	C_s (F/g)	SE (Wh/kg)	SP (kW/kg)	Stability		Ref
							Cycles	Retention %	
NiS	Symmetric	PVA-$LiClO_4$	1.4	56 at 10 mV/s	9.30	0.67	1500	90	[58]
MnO_2	Symmetric	PVA-$LiClO_4$	1.6	110 At 5 mV/s	23	1.90	2200	92	[59]
rGO-PMo_{12}	Symmetric	PVA-H_2SO_4	1.6	51 at 5 mV/s	17.20	0.13	5000	95	[54]
MoS_2/Carbon cloth	Symmetric	PVA-$LiClO_4$	1.0	368 at 5 mV/s	5.42	0.13	5000	96.5	[60]
AC//$NiTe_2$	Asymmetric	3M KOH	1.6	95 at 1 A/g	-	-	3000	81	[32]
MWCNTs/ $MoSe_2$	Symmetric	PVA-KOH	1.4	27 at 0.4 A/g	7.71	0.68	1000	95	[61]
MWCNTs/ MoS_2	Symmetric	PVA-$LiClO_4$	1.6	22 at 1.5 mA	7.90	0.59	1000	100	[53]
MnS	Symmetric	PVA-KOH	1.2	68 at 3 mA	19	0.15	2000	75	[62]
FeS	Symmetric	PVA-$LiClO_4$	2.0	5 at 0.75 mA	2.56	0.72	1000	91	[34]
Siloxene	Symmetric	0.5M $TEADF_4$	3.0	4 at 0.25 mA	5.08	0.37	10000	98	[63]
Phosphorene and graphene	Symmetric	$BMIMPF_6$	3.0	10 mF/ cm^2 at 5 mV/s	11 mWh/cm^3	1.5 W/cm^3	2000	89	[64]
MXene-AC	Symmetric	Et_4NBF_4/AN	2.0	126 at 0.1 A/g	17.5	0.21	100000	92	[65]
SS/MWCNTs/ $MoTe_2$	Symmetric	PVA-$LiClO_4$	1.4	68 at 0.2 mA/cm^2	18.51	0.41	2000	94	Present report

E-Potential window, C_s- Specific capacitance, SE-Specific capacitance, SP-Specific power

Table 4: Corresponding EIS equivalent circuit parameters of the SS/MWCNTs/$MoTe_2$ FCSS-SC device.

Parameters	R_s (Ω)	C_{dl} (F)	R_{ct} (Ω)	CPE		R_L (Ω)	W
				Q-Y_o ($S \cdot s^{-1}$)	Q-n		
Value	3.01	2.218E-5	18.97	0.001355	0.8	333.8	1.645E-14

R_s-Equivalent series resistance, C_{dl}-Double layer capacitance, R_{ct}-Charge transfer resistance, CPE- Constant phase element, Y_o- Admittance, n- Exponential, R_L- Leakage resistance, W-Warburg resistance

TOC

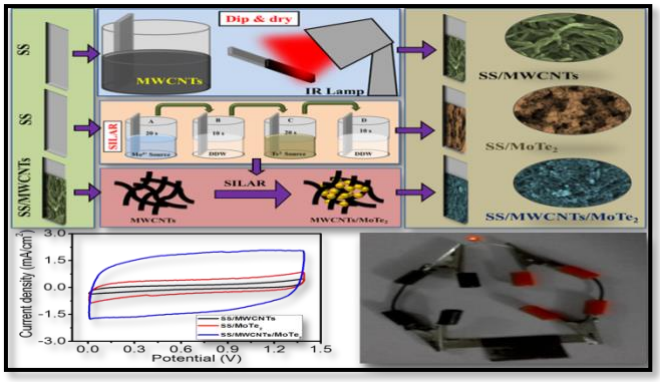

Growth of pseudocapacitive-$MoTe_2$ over EDLC-MWCNTs with enhanced performance through materials mutualism towards flexible solid-state supercapacitor device.